PROCEEDINGS OF SPIE

SPIEDigitalLibrary.org/conference-proceedings-of-spie

Small animal imaging using a curved array photoacoustic tomography system

John Gamelin, Andres Aguirre, Anastasios Maurudis, Fei Huang, Diego Castillo, et al.

John Gamelin, Andres Aguirre, Anastasios Maurudis, Fei Huang, Diego Castillo, Lihong V. Wang, Quing Zhu, "Small animal imaging using a curved array photoacoustic tomography system," Proc. SPIE 6856, Photons Plus Ultrasound: Imaging and Sensing 2008: The Ninth Conference on Biomedical Thermoacoustics, Optoacoustics, and Acousto-optics, 68560Q (28 February 2008); doi: 10.1117/12.769238

SPIE.

Event: SPIE BiOS, 2008, San Jose, California, United States

Small animal imaging using a curved array photoacoustic tomography system

John Gamelin[*a], Andres Aguirre[a], Anastasios Maurudis[a], Fei Huang[a], Diego Castillo[a], Lihong V. Wang[b], and Quing Zhu[a]

[a]Dept. of Electrical Engineering, University of Connecticut, Storrs-Mansfield, CT 06269

[b]Dept. of Biomedical Engineering at Washington University in St. Louis, St. Louis, MO 63130

ABSTRACT

We report experimental imaging results with mice using an array-based photoacoustic tomography system designed for small animal imaging. The system features a 128-element curved transducer array with stage rotation to enable complete two-dimensional tomographic imaging in less than 15 seconds. High fidelity imaging of *ex vivo* mouse brain vasculature was achieved with resolution of vessels less than 200 microns in diameter in the cortex as well as the cerebellum. Images obtained using varying measurement surface angular spans clearly illustrate the impact on feature definition with orientation. The high sensitivity of the system was demonstrated by images of the brain vasculature with an overlying turbid medium (μ_a=0.03 cm^{-1} and μ_s'~7 cm^{-1} at 780 nm) of over 2 cm depth. In phantom experiments, high-quality images of blood tubing in a turbid medium were achieved at depths greater than 3 cm for incident fluences of less than 15 mJ/cm^2. These results illustrate the suitability for near real-time small animal imaging of deep tissue with high definition.

Keywords: Photoacoustic tomography, small animal imaging, phased array ultrasound, optical tomography

1. INTRODUCTION

Interest in small animal imaging has surged in recent years, due in part to the refinement of non-invasive imaging modalities with the requisite resolution and molecular specificity. These methods allow *in vivo* monitoring of disease progression throughout extended longitudinal studies with the control of experimental parameters possible with animal models. To date, most photoacoustic tomographic systems for small animal imaging have adapted early systems used for phantom studies and not incorporated fast imaging technologies or compact instrumentation. As a result, these implementations are not suitable for near real-time *in vivo* imaging as required for functional imaging. Furthermore, variation of physiological parameters during long imaging sessions complicates interpretation and quantitative accuracy of derived optical characteristics.

Ultrasound transducer arrays offer a means for the simultaneous achievement of both fast acquisition and miniaturization. The fixed arrangement of elements precisely aligns transducer measurement positions ensuring exceptional stability and registration with the sample. Most array-based photoacoustic systems have adapted linear or phase-array transducers[1-6], often

Photons Plus Ultrasound: Imaging and Sensing 2008: The Ninth Conference on Biomedical Thermoacoustics, Optoacoustics, and Acousto-optics, edited by Alexander A. Oraevsky, Lihong V. Wang, Proc. of SPIE Vol. 6856, 68560Q, (2008) · 1605-7422/08/$18 · doi: 10.1117/12.769238

modified from commercial systems optimized for imaging of human subjects. The linear geometry of the probe, however, limits achievable angular field-of-view to less than about 90 degrees. The limited view introduces imaging artifacts and prevents detection of high-aspect ratio features (such as blood vessels) oriented perpendicular to the transducer plane[7]. Multiple linear transducers, arranged in an L or square geometry[8], can provide greater angular coverage and improve imaging fidelity.

Curved arrays provide the most suitable configuration for tomographic imaging due to the perfect matching to the cylindrical geometry and elimination of corner effects intrinsic to L- or square-mated linear arrays. Custom curved arrays have been developed for breast cancer applications[9] as well as small animal imaging[10]. The latter system featured a 128-element curved array that, when the sample located at the center of curvature was rotated, formed an open-ended spherical measurement surface for three-dimensional imaging. The system was used for imaging of various organs of sacrificed mice, demonstrating the utility for full-body investigations. Due to the low transducer operating frequency (2.5 MHz), however, resolution of detailed features such as blood vessels within the brain was poor.

In this paper, we present details of the design and characterization of an improved photoacoustic system optimized for tomographic small animal imaging. The system uses a 128-element transducer array and features a higher operating frequency for resolution of fine features such as brain vasculature while retaining high sensitivity for deeper imaging. Complete two-dimensional tomographic scans require less than 15 seconds, enabling pioneering real-time PAT functional studies with small animals.

2. MATERIALS AND METHODS

Experimental Setup

Figure 1 depicts a picture of the experimental configuration. A Ti:Sapphire (Symphotics TII, LS-2134) laser optically pumped with a Q-switched Nd:YAG laser (Symphotics-TII, LS-2122) delivered 8-12 ns pulses at 15 Hz and 780 nm wavelength. The beam was diverged with a plano-concave lens and homogenized by a circular profile engineered diffuser (ED1-S20, ThorLabs, Newton, NJ) to produce a uniform illumination of approximately 50 mm in diameter at the sample. The radiance at the sample was below 15 mJ/cm^2 for all experiments. The laser light was positioned at the center of curvature of a 90-degree annular transducer submerged in a 50-gallon water tank. The light was incident orthogonal to the ring transducer imaging plane for maximum uniformity.

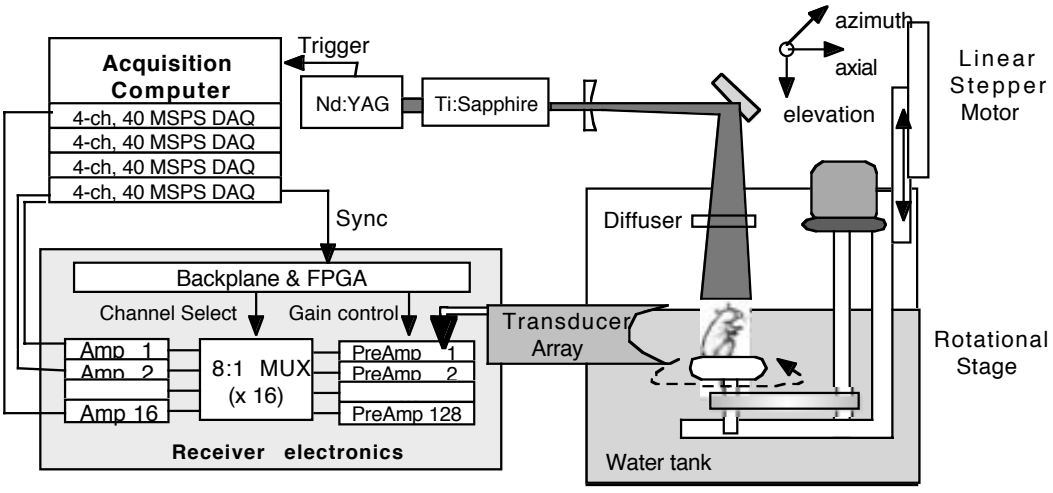

Figure 1. Experimental Setup. A Nd:YAG pumped Ti:Sapphire laser operating at 780 nm and up to 30 mJ is expanded, turned with a mirror, and diffused to a diameters of 12 to 20mm. The beam illuminates the samples orthogonal to the ring transducer array. A rotational stage rotates the samples in 90-degree increments to emulate a full 512-element array.

Details of the transducer design and characterization have been described elsewhere[7]. In brief, the transducer consists of 128 elements arranged along a 90° arc with a 25 mm center of curvature. The array was designed as a building block for a 512 element closed ring system. The array was custom fabricated by Imasonic, Inc. (Besançon, France) using piezocomposite technology for high sensitivity and signal-to-noise ratio. The center frequency of the array was 5 MHz with a reception bandwidth of greater than 60%. Individual elements featured an elevation height of 10mm with an azimuthal pitch of one wavelength (0.308 mm) and kerf of 0.1 mm. The array elements were shaped in the elevation direction to produce an arc-shaped focus at 19 mm from the transducer without the distortions and loss of sensitivity encountered with external acoustic lens materials. In the full 512-element configuration, this focus results in a uniform central imaging region of approximately 16 mm in diameter.

The photoacoustic signals from each element were individually amplified 60 to 70 dB and multiplexed into 16 data acquisition channels sampling at 40 MHz with 12-bit precision. Due to the multiplexing, eight laser firings were required to generate a single 128-channel capture. The data was DMA transferred to RAM and subsequently disk for post-processing.

All samples were mounted on a rotary stage positioned at the radius of curvature that was turned in 90° increments to emulate the response of a full ring. The temperature was continuously monitored with a digital thermometer for precise determination of the sound speed. Without corrections using this measurement, temperature variations throughout the duration of experimentation produced registration errors of up to 500 microns in 360° tomographic imaging. Images were reconstructed using the backprojection algorithm of Xu and Wang[11] using both terms of the kernel (exact backprojection) or the non time-derivative term only (delay-and-sum).

System Photoacoustic Characterization

For small animal tomographic imaging, there are several important performance characteristics: uniformity over the field-of-view, resolution, and sensitivity. In order to evaluate the uniformity over the field-of-view, a short (0.4 mm diameter x 1 mm length) pencil lead was mounted on a clear plastic fiber and scanned across the imaging plane at the center of the transducer elevation. The spacing of measurement locations was 1 mm and for each position the peak absorbed optical energy was estimated using the delay-and-sum algorithm. For comparison, the uniformity was theoretically determined using acoustic reciprocity and the Field II ultrasound simulation program[12].

System resolution was evaluated using both single and dual targets. In both measurements, an 80 μm black thread was suspended at a slight oblique angle to the elevation direction. In the dual target configuration, two strings were fixed with a tapered spacing and translated along the elevation direction at the elevation focal distance for maximum resolution (Figure 3(a)). The resolution was defined as the minimum spacing that provided approximately 10% dip between the two string images.

The sensitivity for realistic tissue imaging was estimated using a 1 cm long polyethylene tube of 580 μm inner diameter filled with blood. The tube was submerged in a 1:4 volume ratio milk:water solution at depths ranging from 3 to 35 mm. The calibrated optical absorption and reduced scattering coefficients of the solution using a frequency domain diffusive optical tomography imager were μ_a=0.03 and μ'_s=7.8 cm^{-1} (typical values for biological tissues) at the 780 nm operating wavelength. The incident fluence was approximately 8 mJ/cm^2 and the system gain was set to 70 dB. The peak-to-peak photoacoustic signal voltage for a single transducer element was monitored for each depth along with complete two-dimensional tomographic images of the tube.

Mouse Vasculature Imaging

Following detailed characterization and investigation of imaging effects with phantoms, the system performance for small animal imaging was evaluated through *ex vivo* imaging of mouse brain vasculature. Axial plane images of brain vasculature have become a widely used standard for demonstration of photoacoustic imaging quality due to the comparatively high contrast and well defined anatomy[13-15]. The mouse brain, however, extends to depths of less than 5 mm. To extend the measurements to evaluate the potential performance with deeper organs in other body sites, additional measurements were performed with an overlying turbid medium to simulate intervening tissue.

Freshly sacrificed 50g white mice were obtained from the University of Connecticut Office of Animal Research. The mice were euthanized according to procedures established by the National Institutes of Health as well as the University Animal Care and Use Committee. The mice were mounted upright in a 1" diameter PVC pipe on the rotational stage with the top of the skull parallel to the imaging plane. Imaging was performed with intact skull and skin using only commercial hair remover lotion for depilitation. For baseline measurements in water, the incident 750 nm beam was expanded and homogenized by an engineered diffuser to a fluence

less than 8 mJ/cm^2. To evaluate the system sensitivity with intervening tissue, the mice were submerged at depths up to 2.5 cm in a 1:5 volume ratio milk:water solution of measured μ_a=0.03 cm^{-1} and μ'_s=5.0 cm^{-1}. For these cases, the beam was expanded to 1.4 cm diameter with an incident fluence of approximately 14 mJ/cm^2. No experimental averaging was performed for all measurements except the 2.5 cm depth for which 16 averages were used for image formation.

3. RESULTS AND DISCUSSION

Uniformity over the field-of-view

Figure 2(a) depicts the measured imaging uniformity over the field-of-view for the quarter ring (90°) configuration. The sensitivity and resolution peaks at the elevation focus located at (19mm – 25 mm = -6 mm). The drop-off in sensitivity is slower towards the ring center due to the contribution of all 128 elements with low directivity angles as opposed to locations in the periphery where the angle between the transducer normal and imaging point exceed 45 degrees. This effect is more pronounced in the full ring simulation depicted in Figure 2(b) that indicates a relative uniformity within 25 % throughout the central 2 x 8 = 16 mm region of the ring. Note that although the sensitivity is uniform throughout the central disk the elevation resolution varies from approximately 600 μm at -6 mm to between 2 and 3 mm at the center due to the mechanical focus in the elevation direction.

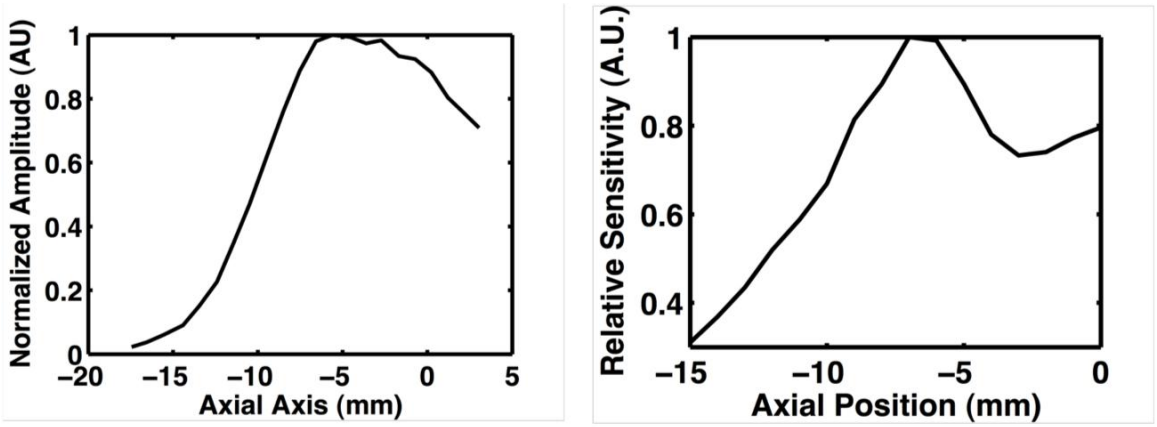

Figure 2. (a) Measured relative sensitivity from the center (0 mm) to the edge (-15 mm) in the axial direction for the quarter ring configuration. (b) Simulated relative sensitivity for the full ring configuration.

Resolution

Figure 3 depicts the two-target resolution measurement images. After subtraction of the 80 μm thread diameter, a resolution of 165 micron was obtained which agrees with the theoretical value for the projected aperture of 35 mm and center frequency of five MHz.

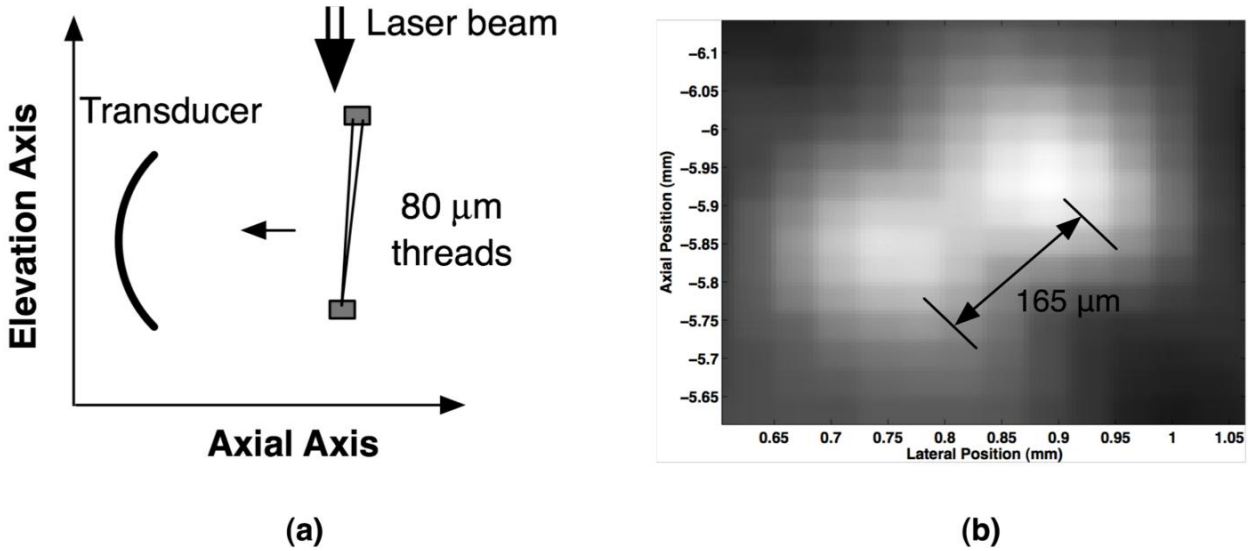

Figure 3. (a) Measurement configuration for the two-target resolution measurement. (b) Image at the resolution limit demonstrating a 165 µm resolution after subtraction of the 80 µm thread diameter.

Sensitivity

The high sensitivity of the system with intrinsic contrast is demonstrated in Figure 4. The peak-to-peak voltage measured for the blood tube falls off exponentially after saturating at shallow depths. Even at 33 mm depth, the single-element SNR exceeds 6 dB with a signal voltage of over 30 mV. The excellent sensitivity results in good contrast exhibited in images obtained at over three cm depth (Figure 4 (b)).

Mouse Vasculature Imaging

Figure 5 presents the images of mouse brain vasculature for an axial cross-section at an intermediate depth within the brain. Excellent definition of primary blood vessels with diameters of 150 µm and larger (as determined independently from microscopy) is observed, demonstrating the high resolution of the system for *in vivo* applications. In particular, the highly regular vascular network in the cerebellum, unresolved in many reported images in the literature, is prominently reproduced with fidelity. Due to the modest transducer frequency, however, some of the microvasculature cannot be resolved.

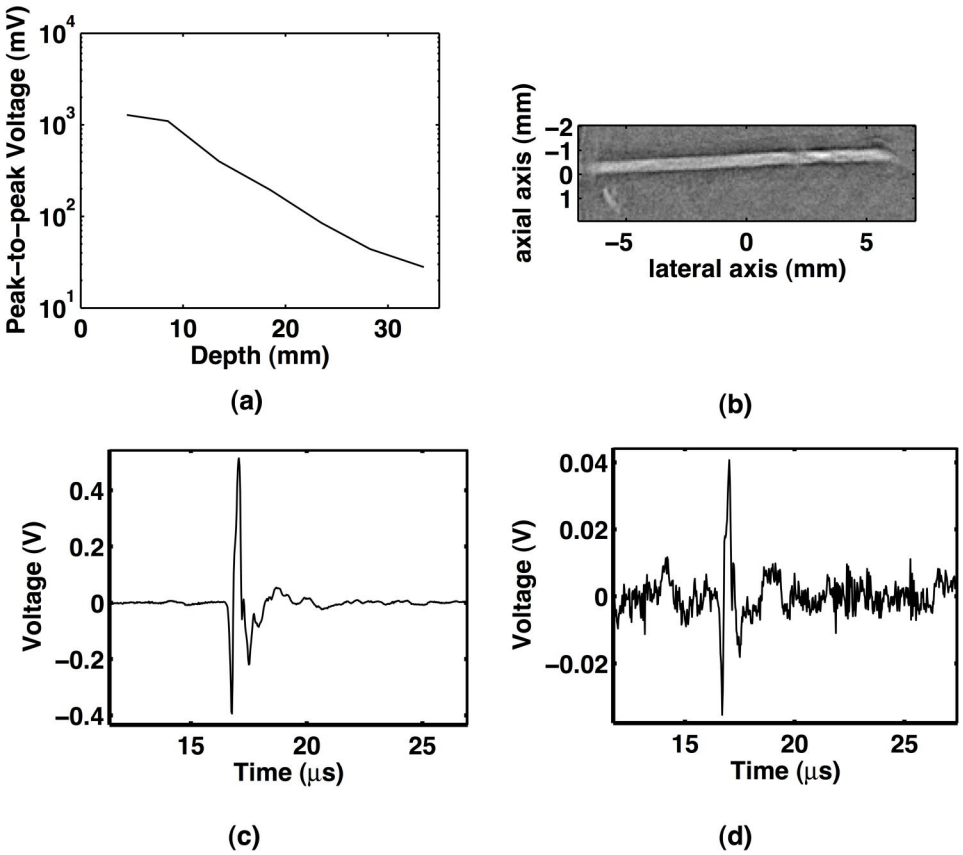

Figure 4. (a) Peak-to-peak single element transducer voltage vs. submersion depth for a blood tube. (b) Backprojection image at 33 mm depth. Single element voltage traces for the tube at 8.5 mm (c) and 33.5 mm (d) depths in the turbid medium. The SNR is still over 6 dB at 33 mm depth.

Although vasculature in the caudal and rostral portions of the brain was resolved, vessels of similar size in the intervening portion of the brain exhibited very poor contrast or were not visible. This is due to their location in the central heavily defocused region of the imaging space (away from elevation focus) so that only the largest veins (e.g. superior sagittal) had sufficient contrast. As discussed earlier, the images include contributions from a depth range of approximately 3 mm near the center to less than 1 mm at the skull edges.

The array of images illustrates the influence of measurement aperture on vasculature definition. With the nominal 90-degree aperture, the only features discernible are those oriented along the azimuth axis, such as the superior sagittal sinuses. Vessels at oblique angles such as the transverse sinuses appear only when the measurement surface increases to 145 or 180 degrees. The symmetric features on the side of the brain away from the transducer are notably reduced in intensity. The lower estimated absorption in these regions may be due to acoustic attenuation from the greater distance or phase mismatches due to local deviations in the brain sound speed from the assumed homogeneous velocity.

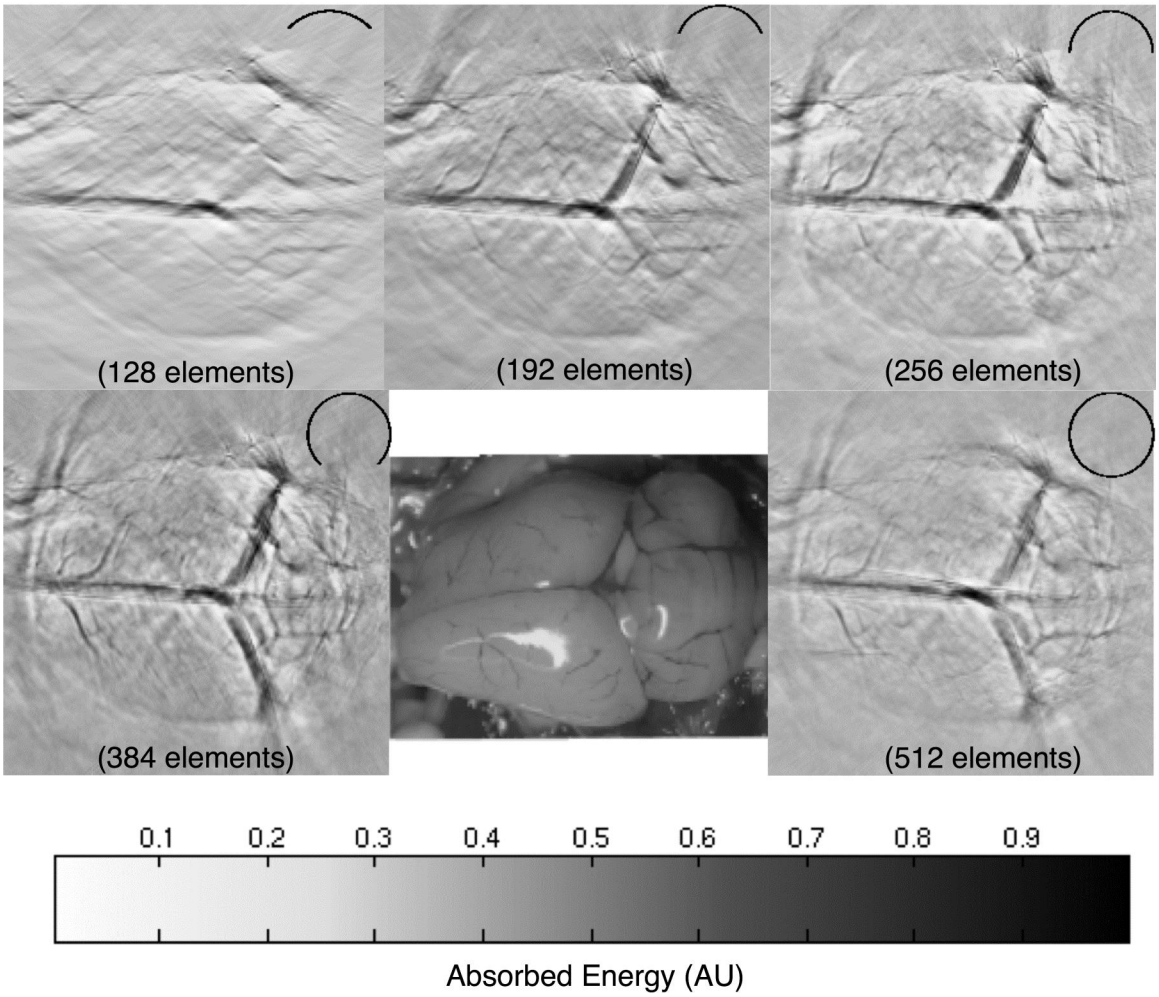

Figure 5. Images of mouse brain vasculature vs. number of elements. The effective angular aperture for each image is depicted in the upper right corners. The open-skull photograph at bottom center highlights vasculature visible from the outermost layers.

Vessels perpendicular to the transducer surface are resolved only when the measurement surface closes to 270 or 360 degrees. Although the definition of all features is excellent for the 270-degree configuration, the relative absorption weighting of individual vessels is not correct. Because of the highly oriented vasculature, the majority of the photoacoustic radiation for the axial features has been measured but approximately half of the generated photoacoustic pressure for the high aspect ratio azimuthal vessels is concentrated in the region corresponding to the final 90 degrees of the measurement surface. As a result, the proper rendition of the relative absorptions requires the full tomographic view as evidenced by the dominance of the confluence of sinuses (where the sinuses drain) over the feeding transverse sinuses.

Figure 6 demonstrates the high sensitivity obtainable with the ring system with an intervening tissue-simulating turbid medium. The mouse used for this imaging session exhibited poorer feature contrast than that of the previous example. A comparison of the baseline water medium image (left side images) with the tissue-simulating medium (center and right side images) reveals that feature detail is preserved to depths greater than 2 cm with modest averaging.

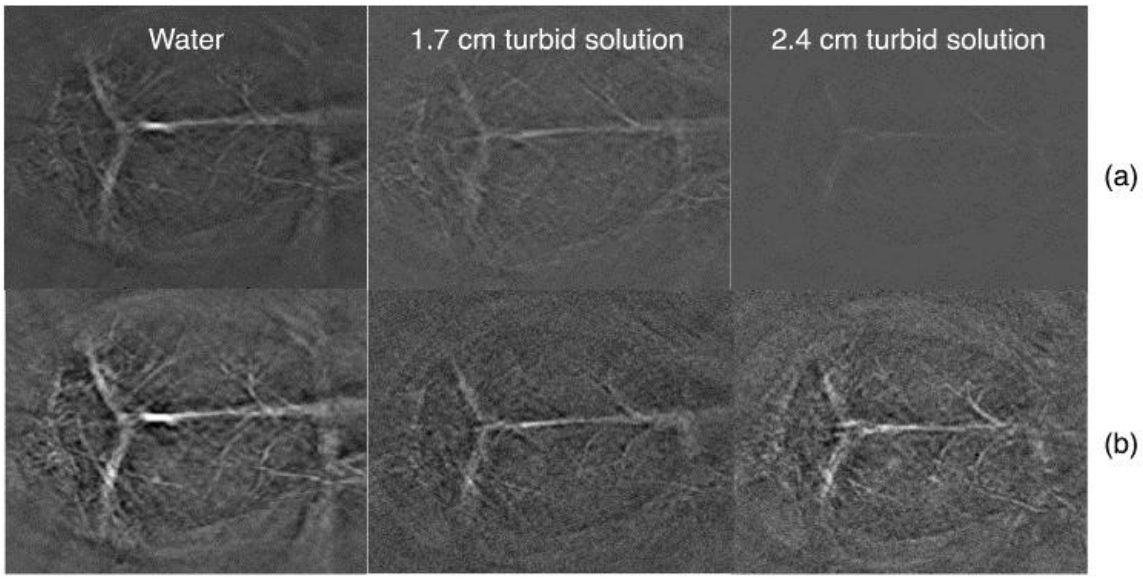

Figure 6. Mouse brain vasculature image comparison with clear and turbid overlying medium of various depths. (a) Images are normalized to an absolute scale to illustrate the loss of signal. (b) Each image is independently normalized to highlight the preservation of vasculature features despite an overall reduction in contrast. Sixteen averages were used for the 2.4 cm depth. No averaging was used for the other two cases.

4. CONCLUSION

In this work, we demonstrated fast, two-dimensional tomographic imaging using an annular transducer array optimized for small animal imaging. With a resolution of 160 μm and full 360-degree view, mouse brain vasculature was imaged with high sensitivity to a tissue-equivalent depth of over 2 cm. Images with increasing measurement aperture illustrated the impact of transducer field-of-view on qualitative and quantitative feature contrast.

5. ACKNOWLEDGMENTS

We acknowledge partial support from NIH grants NIH R01 NS46214 and NIH R01EB002136.
The author can be contacted at (860) 486-3673 or via e-mail at jkg@engr.uconn.edu.

6. REFERENCES

[1]V. Kozhushko, T. Khokhlova, A. Zharinov, I. Pelivanov, V. Solomatin, & A. Karabutov, "Focused array transducer for two-dimensional optoacoustic tomography," J Acoust Soc Am **116(3),** 1498-1506 (2004).

[2]R. A. Kruger, W. L. Kiser, D. R. Reinecke, & G. A. Kruger, "Thermoacoustic computed tomography using a conventional linear transducer array," Med Phys **30(5),** 856-860 (2003).

[3]S. Park, S. Mallidi, A. Karpiouk, S. Alyamov, & S. Emelianov, "Photoacoustic imaging using array transducer," Proc.SPIE **6437,** 643714 (2007).

[4]B. Yin, D. Xing, Y. Wang, Y. Zeng, Y. Tan, & Q. Chen, "Fast photoacoustic imaging system based on 320-element linear transducer array," Phys Med Biol **49(7),** 1339-1346 (2004).

[5]R. J. Zemp, R. Bitton, M. L. Li, K. K. Shung, G. Stoica, & L. V. Wang, "Photoacoustic imaging of the microvasculature with a high-frequency ultrasound array transducer," J Biomed Opt **12(1),** 010501 (2007).

[6]J. J. Niederhauser, M. Jaeger, R. Lemor, P. Weber, & M. Frenz, "Combined ultrasound and optoacoustic system for real-time high-contrast vascular imaging in vivo," IEEE Trans Med Imaging **24(4),** 436-440 (2005).

[7]J. Gamelin, A. Aguirre, A. Maurudis, F. Huang, D. Castillo, L. H. V. Wang et al., "Curved array photoacoustic tomographic system for small animal imaging," J. Biomed Opt 13(2), (2008).

[8]G. Paltauf, R. Nuster, M. Haltmeier, & P. Burgholzer, "Experimental evaluation of reconstruction algorithms for limited view photoacoustic tomography with line detectors," Inverse Problems **23,** S81-S94 (2007).

[9]A. A. Oraevsky & A. Karabutov, "Ultimate sensitivity of time-resolved opto-acoustic detection," Proc. SPIE **3916,** 228-239 (2000).

[10]R. A. Kruger, W. L. Kiser, D. R. Reinecke, G. A. Kruger, & K. D. Miller, "Thermoacoustic molecular imaging of small animals," Molecular Imaging **2(2),** 113-122 (2003).

[11]M. Xu & L. V. Wang, "Universal back-projection algorithm for photoacoustic computed tomography," Phys Rev E Stat Nonlin Soft Matter Phys **71(1 Pt 2),** 016706 (2005).

[12]Gamelin, J., Aguire, A., Maurudis, A., Huang, F., Castillo, D., Wang, L. H. V. et al., "Design and characterization of an array-based photoacoustic imaging system for small animal imaging," in L. H. V. Wang (Ed.), [Photoacoustic Imaging and Spectroscopy], Taylor and Francis(2008).

[13]G. Ku, X. Wang, G. Stoica, & L. V. Wang, "Multiple-bandwidth photoacoustic tomography," Phys Med Biol **49(7),** 1329-1338 (2004).

[14]L. Zeng, X. Da, H. Gu, D. Yang, S. Yang, & L. Xiang, "High antinoise photoacoustic tomography based on a modified filtered backprojection algorithm with combination wavelet," Med Phys **34(2),** 556-563 (2007).

[15]Zhang, E., Laufer, J., & Beard, P., "Three-dimensional photoacoustic imaging of vascular anatomy in small animals using an optical detection system," Proc. SPIE **6437**, 64370S (2007).